Polymer Testing 43 (2015) 123–130

Contents lists available at ScienceDirect

Polymer Testing

journal homepage: www.elsevier.com/locate/polytest

Property modelling

A method for the inverse estimation of the static elastic compressional moduli of anisotropic poroelastic foams – With application to a melamine foam

Christophe Van der Kelen [a], Jacques Cuenca [a, b, *], Peter Göransson [a]

[a] Marcus Wallenberg Laboratory for Sound and Vibration Research, Royal Institute of Technology (KTH), Teknikringen 8, SE-10044, Stockholm, Sweden
[b] Siemens Industry Software, Interleuvenlaan 68, B-3001 Leuven, Belgium

ARTICLE INFO

Article history:
Received 20 January 2015
Accepted 7 March 2015
Available online 14 March 2015

Keywords:
Poroelastic materials
Open-cell foams
Inverse estimation
Anisotropy
Melamine foam

ABSTRACT

This paper presents the application of a method for the characterisation of the static, fully relaxed elastic properties of poroelastic materials. The approach is based on full field measurements of the 3D displacements in a number of points on the faces of the compressed material sample. These are used as targets in an inverse estimation to fit a model of the material to the experimental data. The material is modelled as an orthotropic equivalent solid, whose principal directions are not necessarily aligned with the coordinate system in which the experiments are conducted. The angles of relative orientation accounting for the potential misalignment are estimated, together with the elastic moduli of the material. In addition, the proposed model considers the region of reduced stiffness close to material discontinuities, which has been identified in previous investigations. The method is applied to a melamine foam, which is found to have its lowest stiffness in the direction parallel to the rise direction of the material.

1. Introduction

Porous open-cell foams are often used to increase noise and vibration performance in automotive or aeronautical applications. Their low weight and intrinsic properties make them excellent for sound absorption or enhancement of transmission loss. In addition, poroelastic materials can strongly influence the behaviour of vibrating structures and, in that role, the aspects of anisotropy in the elastic properties can be crucial.

Recent research has shown that several aspects related to the constitutive properties of the solid phase is of critical importance when modelling poroelastic materials under structural excitation [2,3]. State-of-the-art work often assumes that the material is isotropic, simplifying the modelling of the material behaviour considerably [1]. However, a lack of numerical techniques to actually predict the anisotropic material behaviour leaves the value of the results as an open question. Recently, a finite element formulation for modelling the anisotropic behaviour of poroelastic materials has been published [4]. In order for these simulations to yield valuable results, real material data should be used to model the materials.

A growing interest in static elastic characterisation of porous foams comes from recent progress related to the characterisation of the anisotropic Hooke's tensor [7,8]. According to the augmented Hooke's law [9], the Hooke's tensor can be written as a superposition of a fully relaxed, static term, and a term containing the anelastic, frequency-dependent properties of the material. The model in [7,8]

* Corresponding author. Marcus Wallenberg Laboratory for Sound and Vibration Research, Royal Institute of Technology (KTH), Teknikringen 8, SE-10044, Stockholm, Sweden.
E-mail address: jcuenca@kth.se (J. Cuenca).

http://dx.doi.org/10.1016/j.polymertesting.2015.03.006
0142-9418/

relies on the strong simplifying assumption that both terms share the same material symmetry. However, Biot [10] and Dovstam [9] have argued that the static and the dynamic terms of the Hooke's tensor may exhibit different degrees of anisotropy in the general case. Therefore, the two terms of the Hooke's tensor should be characterised separately, and thus a dedicated method for estimating the fully relaxed, static term is required, in order for the previously imposed assumption of collinearity of the elastic and anelastic terms in the augmented Hooke's law to be removed.

As detailed in a review paper by Jaouen et al. [5], state-of-the-art methods allow for the separate characterisation of several elastic moduli of orthotropic or transversely isotropic foams. However, all such methods are based on the assumption that the material natural coordinates are aligned with the coordinate system of the measurement setup.

The purpose of the present paper is to apply a recently proposed method [14] to the characterisation of the static, fully-relaxed elastic properties of the solid frame of a real melamine foam. The method accounts for the possible misalignment of the natural coordinate system of the material with the coordinate system in which the experiment is conducted. An additional aspect which needs to be addressed when characterising a real open-cell foam is the existence of a soft boundary region close to material discontinuities, reported for a melamine foam [12], and for several other open-cell poroelastic materials [13]. Guastavino et al. [12] excluded the possibility that the reduction in stiffness close to foam discontinuities is related to damage incurred to the cell structure, and concluded experimentally that it may be inherent to the material.

The paper is organised as follows. First, the method in [14] is adapted for its application to a real material and, in particular, in order to include the properties of the soft boundary conditions as part of the parameters to be estimated. The method is then applied to the characterisation of a melamine foam and the results are presented and discussed with respect to previous work.

2. Characterisation method

An inverse estimation methodology for the different moduli in the static Hooke's matrix $\mathbf{H}^{(0)}$ of a poroelastic material was developed by the authors in [14]. The data used for the approach consists of a set of measured displacements $\mathbf{u}^{\mathrm{EXP}}$. A material model is constructed to calculate the displacements $\mathbf{u}^{\mathrm{FE}}$ for a set of elastic moduli, which are varied within an optimisation routine until the difference between measured and predicted displacements is minimised. In the present investigation, the displacements $\mathbf{u}^{\mathrm{EXP}} = \{u, v, w\}$ are obtained as the result of a static compression of a cubic sample of material by a distance d between two flat plates, as proposed in [12]. The compression is applied subsequently in all three spatial directions, and the three spatial components of the displacement are extracted at the four exposed faces of the sample. A schematic representation of the measurement setup is given in Fig. 1 for a compression of the material in the z direction. In addition to the measurement of the displacements, the static force needed to compress the material sample by d must be measured for a complete characterisation of the Hooke's matrix.

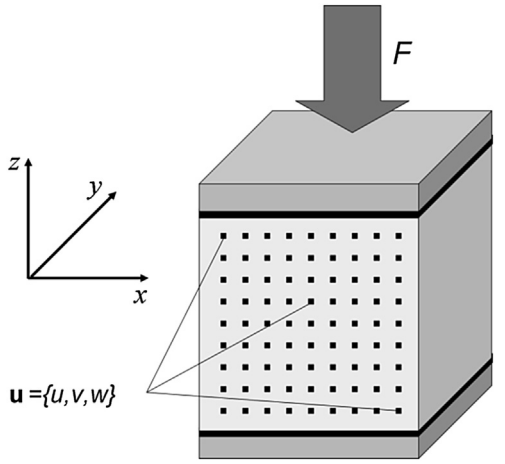

Fig. 1. Representation of the cubic sample (light grey) placed between two rigid plates (dark grey) in the case of a compression along z. The layers of reduced stiffness are shown in black. The dots represent the measurement points.

In the current paper, the objective is to address the application to real materials. This implies that two critical aspects must be addressed in order to characterise the bulk properties of the frame of the poroelastic material. These are the possible, unknown misalignment between the inherent or natural material coordinate system (x, y, z), and the coordinate system (x_a, y_a, z_a) in which the experiments are performed, and the regions of reduced stiffness close to a material discontinuity.

The dimensions of the sample throughout this work are $100 \times 100 \times 100\ \mathrm{mm}^3$. For ease of reference, the different faces of the cubic sample are indicated by their outgoing normal in the coordinate system attached to the sample, x_-, x_+, y_-, y_+, z_-, z_+. The displacement components are defined as $u = (x_0 - x_1)$, $v = (y_0 - y_1)$ and $w = (z_0 - z_1)$, where $\{x_0, y_0, z_0\}$ and $\{x_1, y_1, z_1\}$ are the positions of a point in the material before and after compression, respectively.

2.1. Material model

The foam frame is assumed to have orthotropic material symmetry with its natural coordinate systems not necessarily aligned with the coordinate system attached to the faces of the measured cubic sample. Thus, using Voigt's notation in the measurement coordinate system, the Hooke's matrix consists of 21 non-zero elements, as

$$\mathbf{H}_{\mathrm{a}}^{(0)} = \begin{bmatrix} H_{\mathrm{a},11}^{(0)} & H_{\mathrm{a},12}^{(0)} & H_{\mathrm{a},13}^{(0)} & H_{\mathrm{a},14}^{(0)} & H_{\mathrm{a},15}^{(0)} & H_{\mathrm{a},16}^{(0)} \\ & H_{\mathrm{a},22}^{(0)} & H_{\mathrm{a},23}^{(0)} & H_{\mathrm{a},24}^{(0)} & H_{\mathrm{a},25}^{(0)} & H_{\mathrm{a},26}^{(0)} \\ & & H_{\mathrm{a},33}^{(0)} & H_{\mathrm{a},34}^{(0)} & H_{\mathrm{a},35}^{(0)} & H_{\mathrm{a},36}^{(0)} \\ & & & H_{\mathrm{a},44}^{(0)} & H_{\mathrm{a},45}^{(0)} & H_{\mathrm{a},46}^{(0)} \\ & & & & H_{\mathrm{a},55}^{(0)} & H_{\mathrm{a},56}^{(0)} \\ (\mathrm{sym}) & & & & & H_{\mathrm{a},66}^{(0)} \end{bmatrix} \quad (1)$$

In the natural coordinate system, the Hooke's matrix may be written as $\mathbf{H}^{(0)}$ and $\mathbf{H}_a^{(0)}$ is obtained by rotation

$$\mathbf{H}_a^{(0)} = (\mathbf{A}_\varepsilon^T)^{-1}\mathbf{H}^{(0)}(\mathbf{A}_\varepsilon)^{-1}, \tag{2}$$

where $\mathbf{A}_\varepsilon$ is the Bond matrix of the transformation [15,16] and is given in Appendix A. As a convention, the transformation is defined by three successive rotations around the fixed x, y, and z axes of the natural coordinate system by angles α, β and γ, respectively. The Hooke's matrix $\mathbf{H}^{(0)}$ may then be written in its natural coordinate system in terms of nine independent moduli.

The previously discussed regions of reduced stiffness, which occur at the boundaries connected to the rigid plates, are introduced in the model as a separate top and bottom layer with equivalent isotropic properties, Young's modulus E_{BC} and Poisson ratio υ_{BC}. The foam is thus modelled as a layered material consisting of an isotropic top and bottom layer (black in Fig. 1) and anisotropic properties for the bulk of the material. It is assumed here that the isotropic boundary layers have the same properties for the top and bottom layers in all three directions. The thickness of the boundary layer is derived from an observation of the experimental data.

2.2. Properties to be estimated

The approach developed in [14] stands as a proof of concept where the inverse estimation methodology is numerically validated using fictitious experimental data. The model therein consists of an orthotropic material whose natural coordinates are unknown. This results in 9 elastic moduli and 3 orientation angles, for a total of 12 parameters to be estimated. Additionally, the application of the method to a real material requires the consideration of two more parameters, the Young's modulus and Poisson's ratio of the soft boundary layers, for a total of 14 unknown parameters.

Moreover, as the experimental setup allows measurement of the deformation due to a given compression displacement, a separate setup is required to measure the force required for compressing the sample by distance d. Then, the Hooke's matrix is written in terms of a scaled matrix, as

$$\mathbf{H}^{(0)} = C_H\tilde{\mathbf{H}}^{(0)} = \frac{F^{EXP}}{F^{FE}}\tilde{\mathbf{H}}^{(0)}, \tag{3}$$

where F^{EXP} is the measured force needed to compress the material sample by d, and F^{FE} is its counterpart in the numerical model. C_H is chosen such that $\tilde{H}_{11}^{(0)} = 1$ and determined as detailed later on. This scaling results in a set of 13 parameters to be estimated using the inverse methodology, and one parameter being estimated in an absolute manner.

Furthermore, the different properties to be estimated do not share the same order of magnitude. As a matter of convenience, and to facilitate the inverse estimation process, the components $\tilde{H}_{ij}^{(0)}$ can be written as a multiplication of the normalised components $\widehat{H}_{ij}$ and a set of non-dimensional scaling constants H_{ij}^s, such that $\tilde{H}_{ij}^{(0)} = \widehat{H}_{ij}\cdot H_{ij}^s$, with

$$\widehat{\mathbf{H}} = \begin{bmatrix} 1 & \tilde{H}_{12} & \tilde{H}_{13} & 0 & 0 & 0 \\ & \tilde{H}_{22} & \tilde{H}_{23} & 0 & 0 & 0 \\ & & \tilde{H}_{33} & 0 & 0 & 0 \\ & & & \tilde{H}_{44} & 0 & 0 \\ & (\text{sym}) & & & \tilde{H}_{55} & 0 \\ & & & & & \tilde{H}_{66} \end{bmatrix} \tag{4}$$

and

$$\mathbf{H}^s = \begin{bmatrix} 1 & \xi_3 & \xi_4 & 0 & 0 & 0 \\ & \xi_1 & \xi_5 & 0 & 0 & 0 \\ & & \xi_2 & 0 & 0 & 0 \\ & & & \xi_6 & 0 & 0 \\ & (\text{sym}) & & & \xi_7 & 0 \\ & & & & & \xi_8 \end{bmatrix}. \tag{5}$$

The components of $\widehat{\mathbf{H}}$ are chosen arbitrarily as an initial guess of the properties of the material. Thus, the variables to be estimated are the components of $\mathbf{H}^s$. Similarly, the angles α, β and γ, and the properties of the isotropic boundary layers, E_{BC} being scaled with C_H, and υ_{BC}, are expressed as a multiplication of initial guesses with scaling constants,

$$\begin{aligned} \alpha &= \widehat{\alpha}\,\xi_9, \\ \beta &= \widehat{\beta}\,\xi_{10}, \\ \gamma &= \widehat{\gamma}\,\xi_{11}, \\ \frac{E_{BC}}{C_H} &= \widehat{E}_{BC}\,\xi_{12}, \\ \upsilon_{BC} &= \widehat{\upsilon}_{BC}\,\xi_{13}. \end{aligned} \tag{6}$$

The full optimisation space $\mathbf{x}$ includes the properties of the additional soft layers and thus contains 13 parameters,

$$\mathbf{x} = [\xi_1 \;\; \xi_2 \;\; \xi_3 \;\; \xi_4 \;\; \xi_5 \;\; \xi_6 \;\; \xi_7 \;\; \xi_8 \;\; \xi_9 \;\; \xi_{10} \;\; \xi_{11} \;\; \xi_{12} \;\; \xi_{13}]^T \tag{7}$$

Certain restrictions are imposed on the Hooke's matrix $\mathbf{H}^{(0)}$ by the principle requiring that no energy can be created. This translates into a condition on the Hooke's matrix which must be positive definite, and this is satisfied with the following constraints [17]:

$$\begin{aligned} H_{ii}^{(0)} &> 0, \qquad i = 1, \ldots, 6, \\ g_\sigma(\mathbf{H}^{(0)}) - 1 &= 0, \quad \sigma = 1, \ldots, 4, \end{aligned} \tag{8}$$

where

$$\begin{aligned} g_1 &= \frac{\left(H_{23}^{(0)}\right)^2}{H_{22}^{(0)}H_{33}^{(0)}}, \quad g_2 = \frac{\left(H_{13}^{(0)}\right)^2}{H_{11}^{(0)}H_{33}^{(0)}}, \quad g_3 = \frac{\left(H_{12}^{(0)}\right)^2}{H_{11}^{(0)}H_{22}^{(0)}}, \\ g_4 &= g_1 + g_2 + g_3 - 2\frac{H_{12}^{(0)}H_{23}^{(0)}H_{31}^{(0)}}{H_{11}^{(0)}H_{22}^{(0)}H_{33}^{(0)}} \end{aligned} \tag{9}$$

In addition, the following constraints apply to the angles α, β and γ and the parameters representing the isotropic boundary layer, E_{BC} and υ_{BC},

$$\begin{aligned} -\pi/2 < \alpha, \beta, \gamma < \pi/2 \\ E_{BC} > 0, \\ -1 < \upsilon_{BC} < 1/2. \end{aligned} \tag{10}$$

2.3. Inverse estimation

The objective function used in the optimisation procedure is defined as the square of the absolute difference between the predicted and measured displacements, summed over all faces f in each compression direction c for all points per face N,

$$f(\mathbf{x}) = 1 + A\sum_{c=1}^{3}\sum_{f=1}^{4}\sum_{k=1}^{N}\left|\mathbf{u}_{kfc}^{\mathrm{FE}}(\mathbf{x}) - \mathbf{u}_{kfc}^{\mathrm{EXP}}\right|^2, \tag{11}$$

where a term 1 and a factor $A = 10^3$ are added for numerical stability reasons. The displacements $\mathbf{u}^{\mathrm{FE}}(\xi i) = \{u, v, w\}$ are extracted at the same locations on the material surface as in the experiment. The optimisation routine used is the Globally Convergent Method of Moving Asymptotes (GCMMA), guaranteeing a strict decrease of the objective function [18]. The inverse estimation is considered to have converged to an optimal solution when the variation in the objective function and each of the parameters between two subsequent iterations is less than 10^{-4}.

As a measure of the similarity between simulated and measured displacements, a representation of the difference is given for each compression direction c,

$$\mu_c(\mathbf{x}) = \frac{1}{N}\sum_{f=1}^{4}\sum_{k=1}^{N}\left|\frac{\mathbf{u}_{kfc}^{\mathrm{FE}}(\mathbf{x}) - \mathbf{u}_{kfc}^{\mathrm{EXP}}}{d}\right|, \tag{12}$$

which can be written as a matrix in the form

$$D(\mathbf{x}) = \begin{bmatrix} \mu_{u,x} & \mu_{v,x} & \mu_{w,x} \\ \mu_{u,y} & \mu_{v,y} & \mu_{w,y} \\ \mu_{u,z} & \mu_{v,z} & \mu_{w,z} \end{bmatrix} \tag{13}$$

The component $\mu_{u,x}$, for example, gives the average relative difference on the displacement components u for compression in the x direction over all four faces, relative to the applied displacement d.

3. Application to melamine foam

After the successful verification of the approach in [14], the method is applied to a real foam. Here the measurement method and the preparation of the measurement data are discussed in connection to the characterisation of a melamine foam.

3.1. Experimental setup

The experimental method to acquire the displacements, which are the target data fed into the inverse estimation, is based on a 3D displacement measurement methodology for anisotropic poroelastic cellular foam materials, described in detail in [12]. Using a rotating table, a translating device for purely vertical compression and the image-processing software GOM ARAMIS with two charge-coupled device (CCD) cameras, it is possible to simultaneously obtain the displacements $\mathbf{u}^{\mathrm{EXP}}$ on each of the four faces of the compressed foam. In the current paper, it is assumed that the experimental data is available in a proper format and resolution, as output from the processing done by the system software.

The top and bottom plates used to compress the sample consist of two PMMA plates. These are assumed to be sufficiently stiff such that they apply a uniformly distributed load to the sample and have no influence on the measured data. Double-sided tape was used to glue the plates to the material, and it is assumed that the tape does not allow for sliding of the material. Due to the low stiffness of the melamine foam, the material is very likely to be damaged by removing the PMMA plates. Therefore, it was decided to extract three samples located close to each other in a block of melamine foam, as illustrated in Fig. 2. The rise direction of this block of melamine foam is perpendicular to the x axis. The samples were cut with a thin saw that touches a very small part of the material. As such the surface of the extracted samples remains smooth, and damages to the material were kept to a minimum. The size of each sample is $100 \times 100 \times 100$ mm^3. The density of each sample was measured, and was found to be 9.6, 9.8, 8.4 and 7.9 kg/m^3 for samples 1, 2, 3 and 4, respectively. Sample 1 is loaded in z, sample 2 in y, and sample 3 in x direction. Sample 4 is used in the loading test to determine the factor C_H. An important assumption in the characterisation is that the stiffness properties of the melamine foam block, from which the samples are extracted, are homogeneous.

The applied deformation in the experiment is decided based on considerations in [19], such that the deformation of a poroelastic material is characterised by a linear-elastic regime, thus avoiding collapse of cells due to non-linear elastic buckling in the interior of the foam. An upper limit for the linear-elastic regime in an elastomeric foam in terms of applied displacement is given in [19], a rule of thumb being a deformation of 5%. The samples tested and reported here were compressed 4 mm (4%), which may thus be assumed to be in the linear-elastic regime. After compression, the material was allowed to relax for approximately 8 hours, to achieve a sufficiently relaxed material state.

3.2. Preparation of experimental data

While the experimental results in [12] where presented as displacement on one face of the material, the next step is to combine the measurements of all four faces for one single direction of compression. Fig. 3a shows the measured displacements $\mathbf{u}^{\mathrm{EXP}} = \{u, v, w\}$ of the four faces

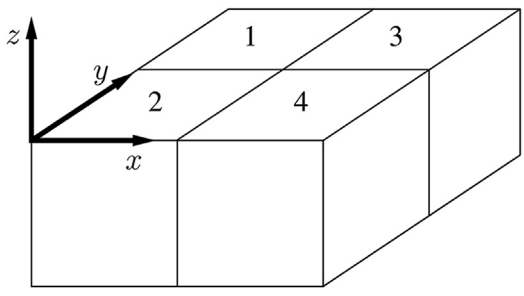

Fig. 2. Orientation of melamine foam samples 1 to 4 in the original material batch.

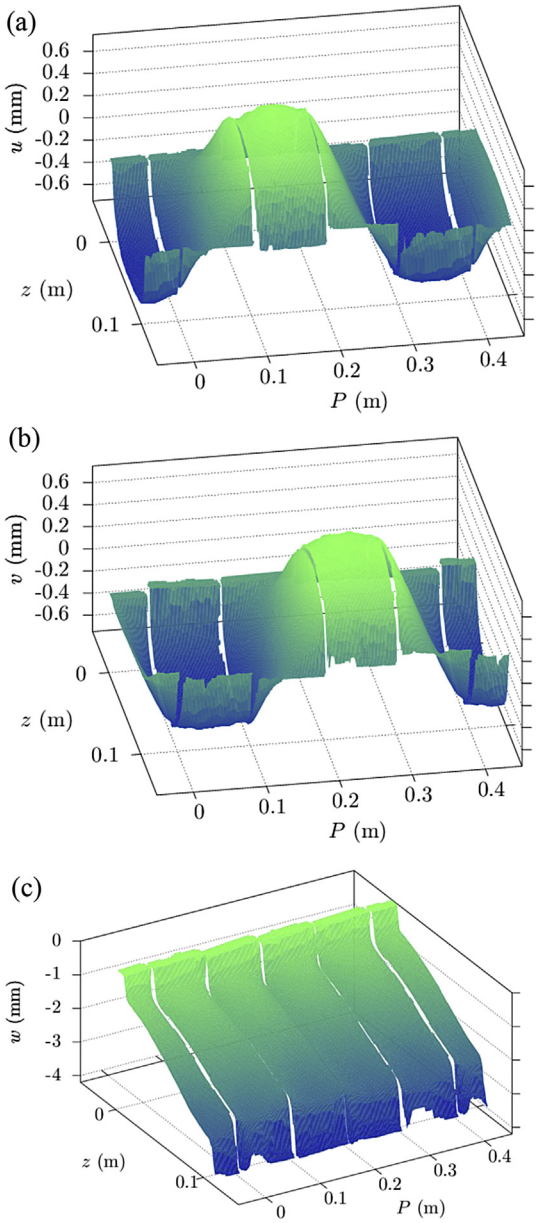

Fig. 3. Deformation of melamine foam under static compression in z by $d = 4$ mm (a) u, (b) v, (c) w.

of sample 1 for compression in the z direction, following the data representation introduced in [14].

In Fig. 3, P is the distance varying along the perimeter of the samples, the faces being represented in the order $[x_-, x_+, y_-, y_+, z_-, z_+]$ such that the edge at $P = 0.4$ m is the same edge as $P = 0$ m. The first and the last faces are repeated to show the continuity over the different edges. The second axis corresponds to the coordinate along which the face is compressed, in this case the z axis, and the vertical axis presents the deformation.

The displacement component w, parallel to the axis of compression, is given in Fig. 3c. It can be seen from the figure that the bottom of the material is indeed immobile ($w = 0$ mm for $z = 0$ m) and a compression of $d = 4$ mm is applied on the top ($w = -4$ mm for $z = 0.1$ m). The regions of reduced stiffness on top and bottom of the material can also be observed. From Fig. 3a and b, the continuity of the displacements over the different edges can be verified, serving as a quality control of the measurements.

The total number of points to be used as target in the inverse estimation depends on the number of points available after processing the images. In order to achieve a good fit, all points available after processing are taken into account in the inverse estimation, resulting in 15812 points for sample 1 (z) and sample 2 (y), and 15008 points for sample 3 (x). The displacements $\mathbf{u}^{FE}$ used in the objective function are extracted at the same coordinates as the displacements $\mathbf{u}^{EXP}$ in the experiment.

3.3. Loading experiment

The actual Hooke's matrix is calculated by multiplication with the factor C_H, detailed in Eq. (3), obtained from the force needed to sustain a compression of 4 mm. The experiment was performed in an INSTRON 4505 testing system with an Interface 1500 load cell. Fig. 4 shows the progress of the applied load on the material in time for such a compression test. The material was first compressed at 0.5 mm/min by 4 mm, to imitate the experiment to obtain the displacements [12], and the applied load was then recorded over a time period of 80 hours. The force decreases continuously, as expected for a visco-elastic material, and reaches a value of 63.38 N after 80 hours, used for the calculation of C_H.

4. Results

The inverse estimation is executed in two phases, as described in more detail in [14]. In the first phase, the material coordinate system orientation angles are not taken into account and a global optimum is found using different starting points. In the second phase, the angles are introduced, with the result that the optimiser converges to different optima for different starting points. To investigate this behaviour further, the second phase of the estimation was performed for 27 different sets of starting points, with all possible combinations of the values $\pi/6 - \pi/6$, and 0 for

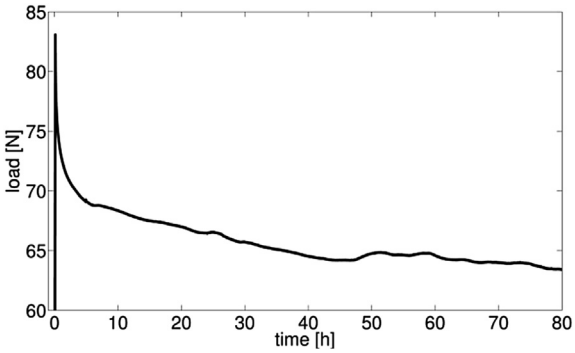

Fig. 4. Change of measured compression force in time for melamine foam sample compressed by $d = 4$ mm.

the angles $\widehat{\alpha}$, $\widehat{\beta}$ and $\widehat{\gamma}$. Five different optimal solutions were found by the optimisation process, of which the three that have the lowest residue of the cost function are discussed here. The other two solutions are in line with the conclusions presented.

The Hooke's matrices $\mathbf{H}_{a}^{(0)}$ for the optimal solutions discussed are

$$\mathbf{H}_{a,1}^{(0)} = \begin{bmatrix} 1.287 & 0.601 & 1.114 & 0.005 & -0.678 & 0.029 \\ & 1.255 & 0.892 & 2.574 & 0.022 & -0.101 \\ & & 3.761 & -2.474 & 0.606 & 0.065 \\ & & & 36.93 & 0.418 & -0.634 \\ & (\text{sym}) & & & 18.45 & 0.579 \\ & & & & & 1.671 \end{bmatrix} (\text{Pa}),$$

$$\mathbf{H}_{a,1}^{(0)} = \begin{bmatrix} 1.222 & 0.604 & 1.08 & -0.165 & -1.374 & -0.185 \\ & 1.376 & 0.978 & 2.534 & 0.333 & -0.242 \\ & & 3.8 & -2.279 & 1.006 & -0.147 \\ & & & 36.81 & 4.887 & -0.495 \\ & (\text{sym}) & & & 37.31 & 1.162 \\ & & & & & 1.096 \end{bmatrix} (\text{Pa}),$$

$$\mathbf{H}_{a,1}^{(0)} = \begin{bmatrix} 1.315 & 0.61 & 1.16 & 0.012 & -0.292 & -0.08 \\ & 1.202 & 1.051 & 0.553 & 0.009 & -0.103 \\ & & 3.656 & -0.456 & 0.235 & -0.073 \\ & & & 7.342 & 0.206 & -0.138 \\ & (\text{sym}) & & & 7.192 & 0.258 \\ & & & & & 0.302 \end{bmatrix} (\text{Pa}), \quad (14)$$

and the corresponding properties estimated for the soft boundary layers are respectively

$$\begin{aligned} E_{BC,1} &= 45.0 \cdot 10^3 (\text{Pa}), \quad \nu_{BC,1} = -0.024, \\ E_{BC,2} &= 44.9 \cdot 10^3 (\text{Pa}), \quad \nu_{BC,2} = -0.027 \\ E_{BC,3} &= 44.9 \cdot 10^3 (\text{Pa}), \quad \nu_{BC,3} = 0.013. \end{aligned} \quad (15)$$

The relative average difference between the displacement for the optimal solutions and the target is obtained from Eq. (13) as

$$D_1 = \begin{bmatrix} 2.42 & 0.98 & 1.80 \\ 1.26 & 2.85 & 1.48 \\ 1.32 & 1.45 & 2.17 \end{bmatrix} (\%),$$

$$D_2 = \begin{bmatrix} 1.91 & 1.23 & 1.95 \\ 1.24 & 3.01 & 1.39 \\ 1.48 & 1.29 & 2.18 \end{bmatrix} (\%), \quad (16)$$

$$D_3 = \begin{bmatrix} 2.17 & 0.97 & 1.69 \\ 1.10 & 3.01 & 1.56 \\ 1.54 & 1.38 & 2.21 \end{bmatrix} (\%),$$

In Fig. 5, the measured and simulated displacements are compared for the solutions discussed. The figures present a snapshot from Fig. 3 for a fixed value of P. Fig. 5a and b show the longitudinal displacement vs the longitudinal dimension, for the middle of face y_+, for compression in the x direction and for the middle of face x_+, for compression in the z direction, respectively. Fig. 5c and d show the lateral displacement vs the longitudinal dimension, for the middle of two opposite faces of the sample, compressed in the x direction. Fig. 5e and f show the lateral displacement vs the longitudinal dimension, for the middle of two opposite faces of the sample, compressed in the y direction.

5. Discussion

Fig. 5 shows that the correlation between measured and predicted data is satisfactory for most faces. From these figures, the difference between the solutions seems to be rather small. The small difference between the solutions is also reflected in the relative average difference between the solution and the measurement, Eq. (16). It is important to note that the comparison is possible under the assumption that the material is homogeneous, since the measurements in the three directions were performed on three different material samples.

The measurement setup used in the present investigation consists of a purely compressional loading of the material. Therefore, as pointed out in previous work [14], the characterisation method allows for a reliable estimation of compressional moduli, while it is weakly sensitive to moduli related to shear and to compression-shear coupling. The present results show a satisfactory agreement between the three solutions in Eq. (14) in the upper left part of the Hooke's matrix (represented in bold), which is related to the compressional moduli of the material. However, the elements of the matrix related to shear show a large variation. This is due to the fact that the particular measurement setup used has a lower sensitivity to shear due to the nature of the deformation applied to the material.

It is worth noting that the solutions obtained exhibit orthotropic symmetry, that is, no higher material symmetry is observed, such as transverse isotropy or isotropy, as assumed in previously existing methods, which would, therefore, be an oversimplifying assumption in the present case.

The results indicate that the present experimental setup yields measured displacements which are very insensitive to changes in the shear moduli, resulting in a very large spread of the terms outside of the upper left part of the Hooke's matrix. Also, the data measured on a real material is not free from flaws, unlike the data for artificial materials studied previously [14]. This suggests that an additional measurement is necessary which clearly activates the shear in real materials to find the Hooke's matrix best representing the poroelastic material. Such a conclusion on the use of compression tests to find the anisotropic material moduli is consistent with the work of Melon et al. [11]. On the other hand, the characterisation of the dynamic Hooke's tensor of porous materials is possible without an explicit shear test [8], due to the existence of compression and shear modes.

Adding the isotropic boundary layers is indispensable for the method to provide a correct fit of the data. Furthermore, these regions are found to have a reduced stiffness compared to the moduli of the main part of the foam, which is especially clear in Fig. 5b.

A final observation, in line with the finding that the material is orthotropic, is that the direction perpendicular to the rise direction has the highest stiffness. This was also found in previous investigations [8] from the characterisation of the dynamic Hooke's matrix of a melamine foam. If a material, such as melamine foam, has been produced in

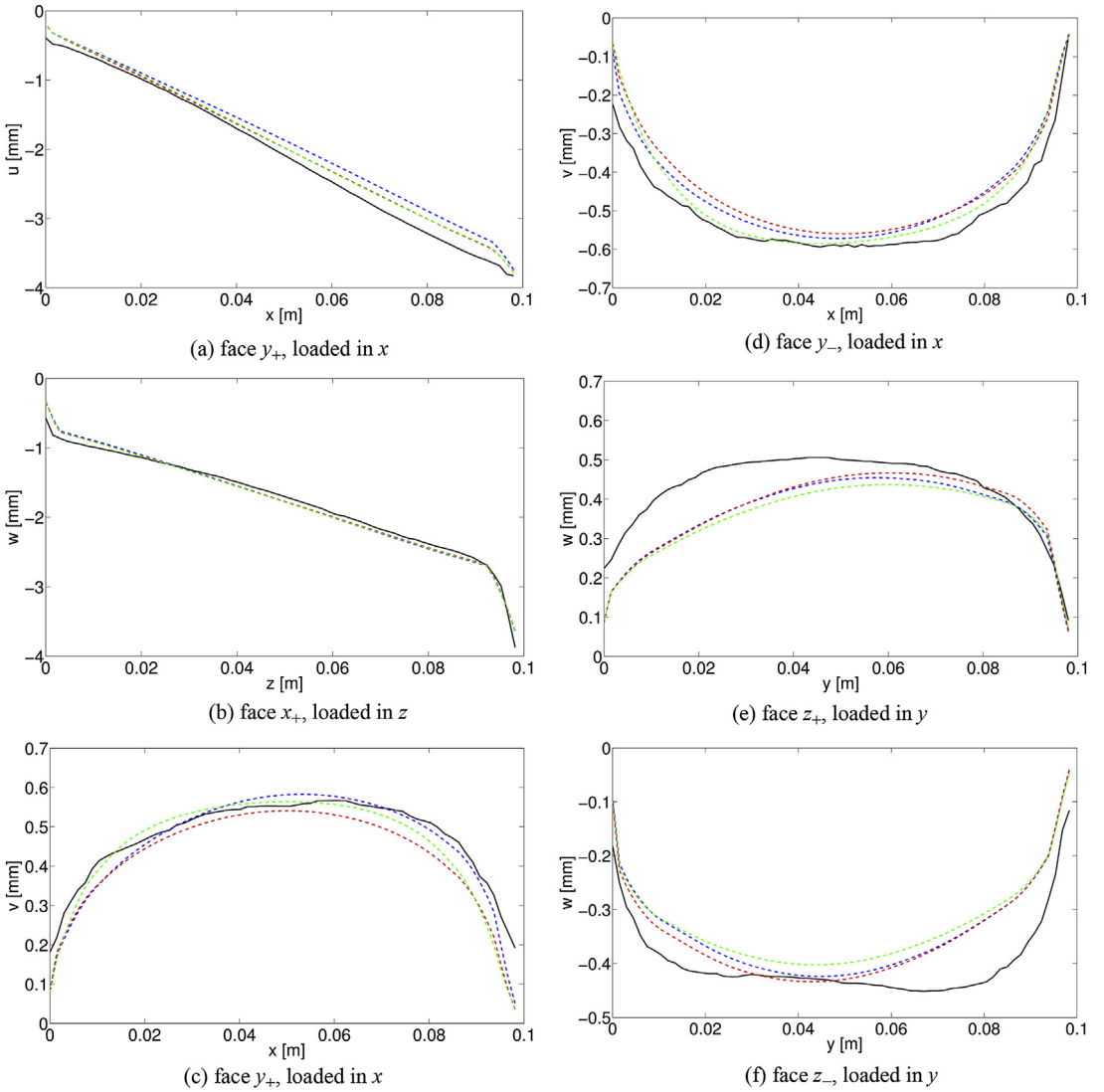

Fig. 5. Comparison between optimal solutions, snapshots of displacement vs longitudinal coordinate on different faces of the material. Black solid line: measurement, blue dashed line: solution 1, red dashed line: solution 2, green dashed line: solution 3. (a) face y_+, loaded in x (b) face x_+, loaded in z. (c) face y_+, loaded in x (d) face y_-, loaded in x. (e) face z_+, loaded in y (f) face z_-, loaded in y.. (For interpretation of the references to colour in this figure legend, the reader is referred to the web version of this article.)

a mould, the cells are usually elongated in the rise direction [19]. A model proposed in [19] for the stiffness moduli of anisotropic poroelastic materials implies that the Young's modulus is generally largest in the rise direction. The results for the present melamine foam seem to contradict this.

6. Conclusions

This paper discusses the application of a proposed method for the characterisation of the static, fully relaxed elastic moduli of open-cell poroelastic materials. The novelty in the proposed approach is twofold. In the first place, the common assumption that the natural axes of the material are aligned with the experimental coordinates is removed, which allows for the characterisation of the full Hooke's matrix with a reduced number of parameters. Second, the boundary condition at material discontinuities for open-cell foams is taken into account by modelling them as isotropic layers with an equivalent Young's modulus and Poisson ratio.

When performing the inverse estimation for a real melamine foam with different starting points, multiple optimal solutions are found. They all give good correlation between the measured and predicted displacements, despite returning very different values for the shear moduli. A closer study of the Hooke's matrices shows that the part of the matrix related to compression is very similar for all solutions, and the terms related to shear or shear-compression coupling are different. It is thus concluded that extending the method proposed in the current paper with a shear test should allow for a full

characterisation of the fully relaxed elastic material parameters.

The values of the observed properties are consistent with measurements using other methods [5]. In particular, the melamine foam shows an orthotropic behaviour. However, the rise direction of the material, as specified by the manufacturer, appears as being aligned with the direction of the lowest modulus.

The method may be combined with the method for the dynamic characterisation of the frame of open-cell poroelastic matetrials [8], and with a method for the characterisation of their static flow resistivity [6], in order to obtain a general constitutive material model to be used in numerical predictions involving anisotropic poroelastic materials [4].

Acknowledgments

The authors would like to acknowledge the support from the European Union, the Smart Structures project (Contract no. MRTN-CT-2006-035559), under which part of the research has been performed. The authors would also like to express their appreciation to Dr. Kent Lindgren and Mr. Danilo Prelević for their precious help with the setup and the experiments, and to the Laboratory of Acoustics and Thermal Physics of KU Leuven for providing the block of melamine foam here tested.

Appendix. Transformation for Hooke's matrix

The Bond matrix for transformation of the Hooke's matrix in Eq. (2) is given by [15,16].

$$\mathrm{A}_{\varepsilon} = \begin{bmatrix} \mathrm{A}_{11} & \mathrm{A}_{12} \\ \mathrm{A}_{21} & \mathrm{A}_{22} \end{bmatrix}, \tag{17}$$

where

$$\mathrm{A}_{11} = \begin{bmatrix} a_{11}^2 & a_{12}^2 & a_{13}^2 \\ a_{21}^2 & a_{22}^2 & a_{23}^2 \\ a_{31}^2 & a_{32}^2 & a_{33}^2 \end{bmatrix},$$

$$\mathrm{A}_{12} = \begin{bmatrix} a_{12}a_{13} & a_{11}a_{13} & a_{11}a_{12} \\ a_{22}a_{23} & a_{21}a_{23} & a_{21}a_{22} \\ a_{32}a_{33} & a_{31}a_{33} & a_{31}a_{32} \end{bmatrix},$$

$$\mathrm{A}_{21} = \begin{bmatrix} 2a_{21}a_{31} & 2a_{22}a_{32} & 2a_{23}a_{33} \\ 2a_{11}a_{31} & 2a_{12}a_{32} & 2a_{13}a_{33} \\ 2a_{11}a_{21} & 2a_{12}a_{22} & 2a_{13}a_{23} \end{bmatrix},$$

$$\mathrm{A}_{22} = \begin{bmatrix} a_{22}a_{33}+a_{23}a_{32} & a_{21}a_{33}+a_{23}a_{31} & a_{21}a_{32}+a_{22}a_{31} \\ a_{12}a_{33}+a_{13}a_{32} & a_{11}a_{33}+a_{13}a_{31} & a_{11}a_{32}+a_{12}a_{31} \\ a_{12}a_{23}+a_{13}a_{22} & a_{11}a_{23}+a_{13}a_{21} & a_{11}a_{22}+a_{12}a_{21} \end{bmatrix} \tag{18}$$

The entries a_{ij} are the elements of transformation matrix $\mathbf{A}_{\varepsilon}$, defined by a successive rotation around the fixed x, y, and z axes of the natural coordinate system by angles α, β and γ respectively,

$$\mathbf{a} = \mathbf{R}_z(\gamma)\mathbf{R}_y(\beta)\mathbf{R}_x(\alpha) = \begin{bmatrix} a_{11} & a_{12} & a_{13} \\ a_{21} & a_{22} & a_{23} \\ a_{31} & a_{32} & a_{33} \end{bmatrix}, \tag{19}$$

with

$$\mathrm{R}_x(\alpha) = \begin{bmatrix} 1 & 0 & 0 \\ 0 & \cos\alpha & \sin\alpha \\ 0 & -\sin\alpha & \cos\alpha \end{bmatrix},$$

$$\mathrm{R}_y(\beta) = \begin{bmatrix} \cos\beta & 0 & -\sin\beta \\ 0 & 1 & 0 \\ \sin\beta & 0 & \cos\beta \end{bmatrix}, \tag{20}$$

$$\mathrm{R}_z(\gamma) = \begin{bmatrix} \cos\gamma & \sin\gamma & 0 \\ -\sin\gamma & \cos\gamma & 0 \\ 0 & 0 & 1 \end{bmatrix}$$

References

[1] J. Allard, N. Atalla, Propagation of Sound in Porous Media: Modelling Sound Absorbing Materials 2e, Wiley, 2009.
[2] C. Van der Kelen, P. Göransson, B. Pluymers, W. Desmet, On the influence of frequency-dependent elastic properties in vibro-acoustic modelling of porous materials under structural excitation, Journal of Sound and Vibration 333 (2013) 6560–6571.
[3] P. Göransson, N.E. Hörlin, Vibro-acoustics modelling of anisotropic porous elastic materials. A preliminary study of the influence of anisotropy on the predicted performance in a multi-layer arrangement, Acta Acustica United with Acustica 96 (2010) 258–265.
[4] N.E. Hörlin, P. Göransson, Weak, anisotropic symmetric formulations of Biot's equations for vibro-acoustic modelling of porous elastic materials, International Journal for Numerical Methods in Engineering 82 (2010) 1519–1540.
[5] L. Jaouen, A. Renault, M. Deverge, Elastic and damping characterizations of acoustical porous materials: available experimental methods and applications to a melamine foam, Applied Acoustics 69 (2008) 1129–1140.
[6] C. Van der Kelen, P. Göransson, Identification of the full anisotropic flow resistivity tensor for multiple glass wool and melamine foam samples, Journal of the Acoustical Society of America 134 (2013) 11.
[7] J. Cuenca, P. Göransson, Inverse estimation of the elastic and anelastic properties of the porous frame of anisotropic open-cell foams, Journal of the Acoustical Society of America 132 (2012) 621–629.
[8] J. Cuenca, C. Van der Kelen, P. Göransson, A general methodology for inverse estimation of the elastic and anelastic properties of anisotropic open-cell porous materials – with application to a melamine foam, Journal of Applied Physics 115 (2014) 084904.
[9] K. Dovstam, Augmented Hooke's law based on alternative stress relaxation models, Computational Mechanics 26 (2000) 90–103.
[10] M.A. Biot, Theory of stress-strain relations in anisotropic viscoelasticity and relaxation phenomena, Journal of Applied Physics 25 (1954) 1385–1391.
[11] M. Melon, E. Mariez, C. Ayrault, S. Sahraoui, Acoustic and mechanical characterization of anisotropic open-cell foams, Journal of the Acoustical Society of America 104 (1998) 2622–2627.
[12] R. Guastavino, P. Göransson, A 3D displacement measurement methodology for anisotropic porous cellular foam materials, Polymer Testing 26 (2007) 711–719.
[13] A. Geslain, O. Dazel, J.-P. Groby, S. Sahraoui, W. Lauriks, Influence of static compression on mechanical parameters of acoustic foams, Journal of the Acoustical Society of America 130 (2011) 818–825.
[14] C. Van der Kelen, J. Cuenca, P. Göransson, A method for characterisation of the static elastic properties of the porous frame of orthotropic open-cell foams, International Journal of Engineering Science 86 (2015) 44–59.
[15] M.A. Slawinski, Waves and Rays in Elastic Continua, second ed., World Scientific Publishing Company, 2010, 616 pages.
[16] J.M. Carcione, Wave Fields in Real Media: Wave Propagation in Anisotropic, Anelastic, Porous Media and Electromagnetic Media, second ed., Elsevier Science, 2007, 515 pages.
[17] R.M. Jones, Mechanics of Composite Materials, Taylor and Francis, Philadelphia, 1999, 519 pages.
[18] K. Svanberg, A class of globally convergent optimization methods based on conservative convex separable approximations, SIAM Journal of optimization 12 (2002) 555–573.
[19] L.J. Gibson, M.F. Ashby, Cellular Solids – Structure and Properties, second ed., Cambridge University Press, Cambridge, 1997, 510 pages.